

Reaction morphology and the effect of pH on the preparation of TiO₂ nanoparticles by a sol-gel method

Chang Sung Lim^a, Jeong Ho Ryu^{b,*}, Do-Hwan Kim^c, Sung-Yong Cho^c and Won-Chun Oh^a

^aDepartment of Advanced Materials Science & Engineering, Hanseo University, Seosan 356-706, Korea

^bR&D Institute, Samsung LED Co., LTD., 314, Maetan3-dong, Yeongtong-gu, Suwon 443-743, Korea

^cDepartment of Environmental Engineering, 77 Yongbong-ro, Buk-gu, Gwangju 500-757, Korea

Titanium dioxide nanoparticles were prepared by hydrolysis of titanium tetra-isopropoxide. Aqueous solutions with various pH and the resultant reaction morphology on the preparation of TiO₂ nanoparticles were investigated. The influence of pH on the reaction morphology of using a titanium tetra-isopropoxide was evaluated depending on the amounts of the catalysts such as HCl and NH₄OH. The morphology and phase transformation of TiO₂ particles prepared by the hydrolysis of titanium tetra-isopropoxide were strongly influenced by the presence of the catalysts. In the case of using NH₄OH, the morphology of the TiO₂ particles exhibited a powder form. In the case of using HCl, it showed a bulk or granular form. The phase transformations of amorphous Ti(OH)₄ to anatase TiO₂ and the anatase to rutile were significantly influenced by the type and the amount of the catalysts.

Key words : TiO₂ nanoparticle, hydrolysis, TTIP, pH, reaction morphology.

Introduction

Nanosized TiO₂ has attracted increasing attention in the scientific community for its wide applications in photocatalysts, solar cells, gas sensors and optoelectronic devices [1, 2]. The applications of TiO₂ arise primarily from its physicochemical properties, such as crystalline structure, particle size, specific surface area, porosity and thermal stability. Controllable synthesis of nanosized TiO₂ particles with these properties, especially crystalline structure, represents some of the key subjects in its applications. In recent years, semiconductor photocatalysis has attracted a great deal of research attention due to its potential application to solve environmental problems [3-5]. Among the various semiconductors employed, TiO₂ is versatile material and good photocatalyst for the degradation of environmental contaminants due to its high photocatalytic activity, absence of toxicity, relatively low cost, and excellent chemical stability under various conditions [6-8]. The excellent photocatalytic property of TiO₂ is due to its wide band gap and the long lifetime of photogenerated holes and electrons. With an appropriate light source, a TiO₂ photocatalyst generates electron/hole pairs to initiate a series of chemical reactions that eventually mineralize the pollutants [9, 10].

TiO₂ usually exists in the form of anatase, rutile and brookite. In a photocatalytic study, anatase TiO₂ is generally considered to be more active than rutile crystalline [11].

The anatase phase is thermodynamically metastable and easily transforms into the stable rutile phase, however, when TiO₂ is calcined at high temperature. Moreover, anatase TiO₂ with a higher crystallinity means fewer defects for the recombination of photogenerated electrons and holes [12]. Rutile TiO₂ has been shown to be negligibly photoactive for the photo-oxidation of many organic pollutants in aqueous media, but its resistance to disaggregation is higher than that of anatase TiO₂ [11, 12].

The increase of the lifetime of the photo-produced pairs, due to hole and electron transfer between the two coupled semiconductors, is invoked in many cases as the key factor for the improvement of the photoactivity. Nevertheless, it should be considered that photoactivity also strongly depends on bulk and surface physicochemical properties of the photocatalysts, such as the type of phases, the surface hydroxylation, the porosity, the surface area, the adsorption capacity, the distribution of the supported photoactive component, and the surface acid-base properties [13-15]. The physical, chemical, and photochemical properties of TiO₂ nanoparticles are dependent on the manufacturing method. To enhance the application of TiO₂, several processes have been developed over the last decade and can be classified as liquid process sol-gel [16-21], solvothermal [22, 23], hydrothermal [24-26], solid state processing routes (mechanical alloying/milling) [27-30], thermal hydrolysis [31, 32] and other routes such as laser evaporation [33], and ultrasonic synthesis [34]. However, TiO₂ particles prepared by these processes are relatively large with inhomogeneous morphologies. From the above methods, the sol-gel method is normally used for the preparation of nanosized TiO₂ particles. The sol-gel process has notable advantages

*Corresponding author:
Tel : +82-31-2103089
Fax: +82-31-3007900(#3466)
E-mail: jimihen.ryu@samsung.com

such as high purity, good uniformity of the microstructure, low temperature synthesis, easily controlled reaction conditions, and hence has been widely adopted for preparing nanostructured TiO₂ particles.

There are several parameters for controlling the sol-gel process to prepare TiO₂ particles with significant properties. It has been demonstrated that the precursor's concentration of precursor titanium alkoxide greatly affects the crystallization behavior and the characteristics of the final particle [35-37]. The size, stability, and morphology of the sol produced from alkoxide is strongly affected by the hydrolysis and pH. The pH of the prepared solution has a great influence on the final size of TiO₂ nanoparticles [38-42]. The reaction morphology and the effect of the pH on the formation of TiO₂ particles is of great interest, because nanosized particles are formed under these conditions. Therefore, a controlled pH and reaction morphology are required for the optimization of the preparation conditions of TiO₂.

In this study, TiO₂ nanoparticles were prepared by the sol-gel route using titanium tetra-isopropoxide. The reaction morphology was investigated depending on the amounts of HCl and NH₄OH, and the effect of the pH on the preparation of TiO₂ nanoparticles was studied. Subsequently, the phase transformations of amorphous Ti(OH)₄ to anatase TiO₂ and anatase to rutile was investigated in detail.

Experimental

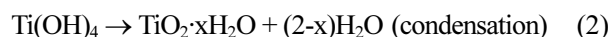
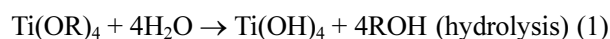
Titanium tetra-isopropoxide (TTIP, Ti(OCH(CH₃)₂)₄) and isopropyl alcohol (IPA, C₃H₈O) were mixed in the molar ratio of 1 : 10 and stirred for 1 hour. Another solution was prepared from a mixture of H₂O and IPA with a molar ratio of 10 : 1. This solution was then titrated into the TTIP-IPA solution and stirred for 2 h until a uniform colloidal TiO₂ sol was produced. A TiO₂ sol is chemically very unstable in the neutral pH range and therefore it easily agglomerates when it transforms into the gel state. However, this instability can be controlled by adding an acid. Solutions with various pH were used as the hydrolysis catalyst. The desired pH value of the solution was adjusted by adding HCl and NH₄OH. The gel preparation process started when both solutions were mixed together under vigorous stirring. After the peptization process, the volume of the solution decreased and a suspension was produced. Depending on the preparation conditions, the resultant suspension was white-blue or opaque with a high viscosity. The viscous solution was dried at 100 °C in an oven for 24 h. After being washed with ethanol and dried at 100 °C in an oven for 10 h, a yellow-white powder was obtained. Finally, the prepared powder was heat-treated at temperatures ranging from 200 to 600 °C for 3 h.

Several techniques were employed for characterization of the powders. The crystallization process of the precursor was evaluated by thermogravimetry-differential thermal analysis (TG-DTA, SETRAM, France), using a sample weight of about 24 mg and a heating rate of 10 °C/min.

The crystalline phases and average crystallite sizes after heat-treatment were identified by powder X-ray diffraction (XRD, CuK_α, 40 kV, 30 mA, Rigaku, Japan) with a scan rate of 3 °C/min. The particle size and microstructural morphology of the nanocrystalline powders were observed by scanning electron microscopy (SEM, JSM-35CF, JEOL).

Results and Discussion

The preparation of the TiO₂ colloids in the nanometre range can be effectively conducted through the hydrolysis and condensation of titanium alkoxides in aqueous media. In the presence of water, alkoxides are hydrolysed and subsequently polymerized to form a three-dimensional oxide network. These reactions can be schematically represented as follows:



where R is ethyl, i-propyl, n-butyl, etc. [43]. It is well known that the tetravalent cations are too acidic so that the nucleation of the stable hydroxide Ti(OH)₄ cannot occur. Water molecules formed according to reaction (2) always bear a positive partial charge. Therefore, oxolation and ololation can proceed simultaneously during nucleation and growth leading to an amorphous oxide TiO₂·nH₂O where the number n of water molecules depends on the experimental conditions. Depending on the experimental procedure, the precipitation of TiO₂ leads to rutile or anatase phases [44, 45]. The stage of deoxilation prior to ololation can be controlled by adjusting the pH and initial water concentration. This control leads to precipitation of anatase nanoparticles of TiO₂ in the experimental procedure.

Table 1 shows the effect of catalysts of NH₄OH/HCl, the molar ratio of catalyst/TTIP, and pH on the morphology and crystalline structure of the TiO₂. When the catalyst is NH₄OH or there is none in the solution with the pH level from 10.07 to 5.04, powder forms with amorphous

Table 1. Effect of catalysts of NH₄OH/HCl, the molar ratio of catalyst/TTIP, and pH on the morphology and crystalline structure of the TiO₂

samples	catalyst	molar ratio catalyst/TTIP	pH	morphology	crystal structure
N 1.0	NH ₄ OH	1.0	10.07	powder	amorphous
N 0.5	NH ₄ OH	0.5	9.45	powder	amorphous
N 0.25	NH ₄ OH	0.25	7.77	powder	amorphous
N 0.0	no catalyst	0.0	5.04	powder	amorphous
H 0.05	HCl	0.05	3.96	agglomerate	amorphous
H 0.1	HCl	0.1	2.95	granule	amorphous
H 0.25	HCl	0.25	2.12	bulk	anatase
H 0.5	HCl	0.5	1.90	bulk	anatase

phases were observed. Otherwise, when the catalyst is HCl in the solution with the pH level from 3.96 to 1.9, an agglomerated granular and bulk form with amorphous and anatase phases were observed. Therefore, TiO₂ nanoparticles with various morphologies and crystal structures were synthesized by the hydrolysis reaction of titanium tetra-isopropoxide using the molar ratio of catalyst and TTIP with various pH values in acid and base solutions. The morphology and phase transformation of TiO₂ powder prepared by hydrolysis of titanium tetra-isopropoxide were strongly influenced by the presence of the catalysts HCl and NH₄OH.

Fig. 1 shows SEM micrographs of the TiO₂ powders dried at 100 °C with NH₄OH as the base catalyst or none. The TiO₂ powder exhibited a homogeneous spherical morphology and a particle size distribution with sizes of 100–200 nm for pH 10.67 in Fig. 1(a) and 9.45 in Fig 1(b). The particle morphology and particle size distribution had an inhomogeneous tendency to decrease depending on a relatively lower pH value of 7.77 in Fig. 1(c) and 5.04 in Fig 1(d). On the other hand, Fig. 2 shows SEM

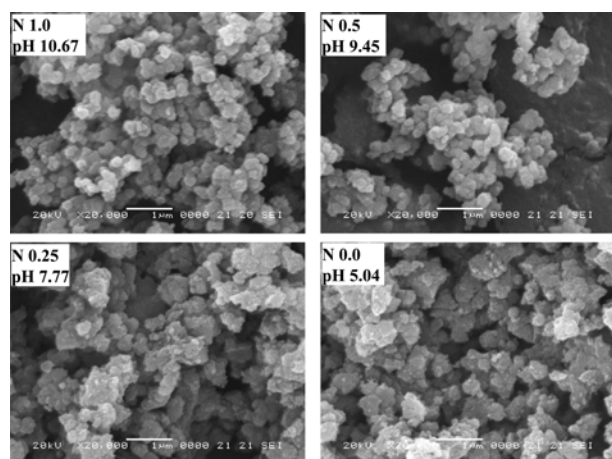


Fig. 1. SEM micrographs of the TiO₂ powders dried at 100 °C with NH₄OH as the catalyst or none; (a) pH 10.67, (b) pH 9.45, (c) pH 7.77 and (d) pH 5.04.

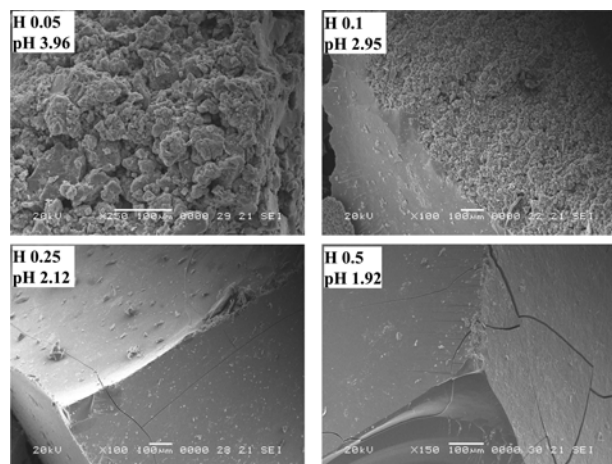


Fig. 2. SEM micrographs of the TiO₂ powders dried at 100 °C with HCl as the catalyst; (a) pH 3.96, (b) pH 2.95, (c) pH 2.12 and (d) pH 1.92.

micrographs of the TiO₂ powders dried at 100 °C with HCl as the catalyst. It showed a granular form for pH 3.96 in Fig 2(a) and a bulk-like form for pH 2.95(b), 2.12(c), 1.92(d).

The effect of pH on the TiO₂ nanopowder after heat-treatment was evaluated for the crystalline phase and size. Fig. 3 shows XRD patterns of TiO₂ powders calcined for 3 h at (a) 200, (b) 300, (c) 400 and (d) 500 °C with NH₄OH as the catalyst; (A) NH₄OH/TTIP = 0.5, (B) NH₄OH/TTIP = 0.25. The representative (101) plane diffraction peak at 25.3° is used for anatase and (110) peak at 27.5° for rutile. This shows that the anatase phase was observed above 200 °C, while the rutile phase above 500 °C. In the case of (A) NH₄OH/TTIP = 0.5 (pH 9.45), the rutile phase was increased compared to the case of (B) NH₄OH/TTIP = 0.25 (pH 7.77) in Fig. 3. The effect of calcination temperature on the crystallization with HCl as the catalyst was also investigated. Fig. 4 shows XRD patterns of TiO₂ powders calcined for 3 h at (a) dried, (b) 200, (c) 300 and (d) 400 and (e) 500 °C with HCl as the catalyst; (A) HCl/TTIP = 0.25, (B) HCl/TTIP = 0.5 in Fig. 4. It shows that the anatase phase was observed above 100 °C and the rutile phase was observed above 500 °C in the case of (A) HCl/TTIP =

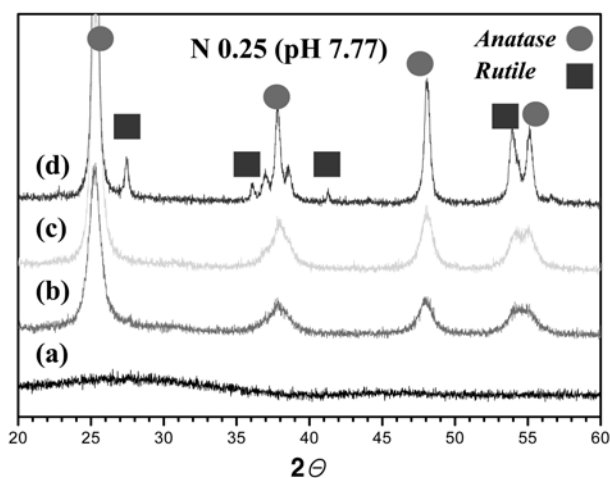
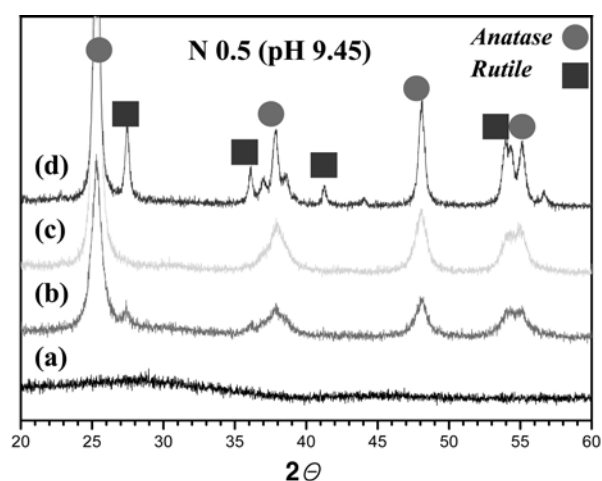


Fig. 3. XRD patterns of TiO₂ powders calcined for 3 h at (a) 200, (b) 300, (c) 400 and (d) 500 °C with NH₄OH as the catalyst; (A) NH₄OH/TTIP = 0.5, (B) NH₄OH/TTIP = 0.25.

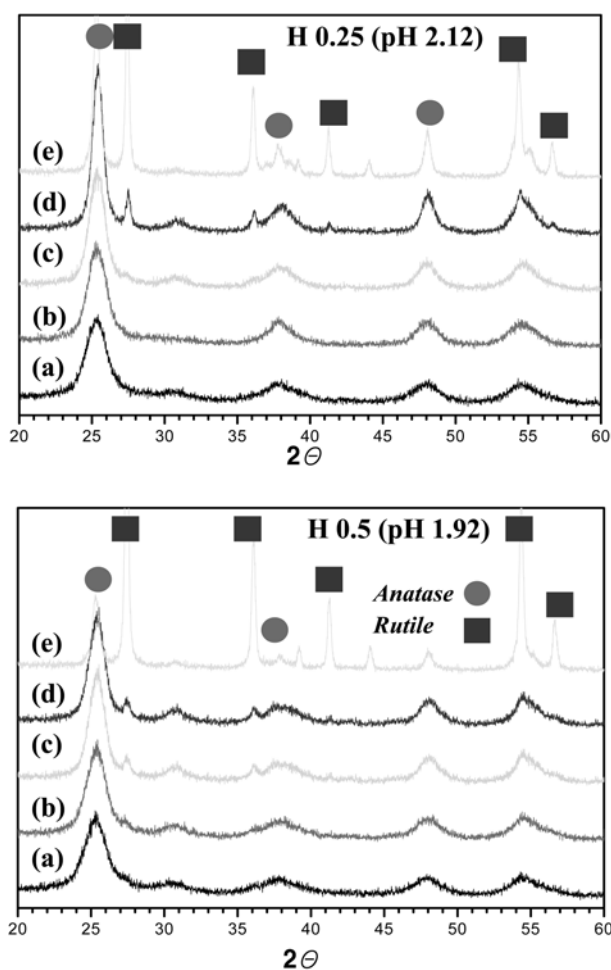


Fig. 4. XRD patterns of TiO₂ powders calcined for 3 h at (a) dried, (b) 200, (c) 300 and (d) 400 and (e) 500 °C with HCl as the catalyst; (A) HCl/TTIP = 0.25, (B) HCl/TTIP = 0.5.

0.25(pH 2.12), while the rutile phase was increased above 400 °C in the case of (B) HCl/TTIP = 0.5(pH 1.92) in Fig. 4.

Table 2 shows the formation of various phases for the TiO₂ powders as a function of pH and the calcination temperature (Am : amorphous, A : anatase, R : rutile). When the temperature was raised, the anatase phase transformed to the rutile phase, which could be attributed to the thermally-promoted crystallite growth. In particular, the phase transformation of amorphous Ti(OH)₄ to anatase TiO₂ and anatase to rutile were significantly activated by the HCl catalyst. On the other hand, the phase transformation and the crystallization of the particles were not activated by the NH₄OH catalyst. This reveals that nucleation and growth of the rutile phase have been initiated at temperatures somewhere from 400-600 °C. It may be assumed that the growth of rutile crystallization was affected by the pH value of acid.

Fig. 5 shows the average calculated weight fractions of anatase as a function of the calcination temperature. The existing phase in the powder after heat-treatment was identified by XRD. The weight fraction of rutile in the powders was estimated in the following equation [46].

Table 2. Formation of various phases for the TiO₂ powders as a function of pH and calcination temperature

sample	pH	dried	200	300	400	500
N 1.0	10.07	Am	Am	A	A	A + R
N 0.5	9.45	Am	Am	A	A	A + R
N 0.25	7.77	Am	Am	A	A	A + R
N 0.0	5.04	Am	Am	A	A	A + R
H 0.05	3.96	Am	Am	A	A	A
H 0.1	2.95	Am	Am	A	A	A
H 0.25	2.12	A	A	A	A + R	A + R
H 0.5	1.90	A	A	A + R	A + R	A + R

*Am : amorphous, A : anatase, R : rutile

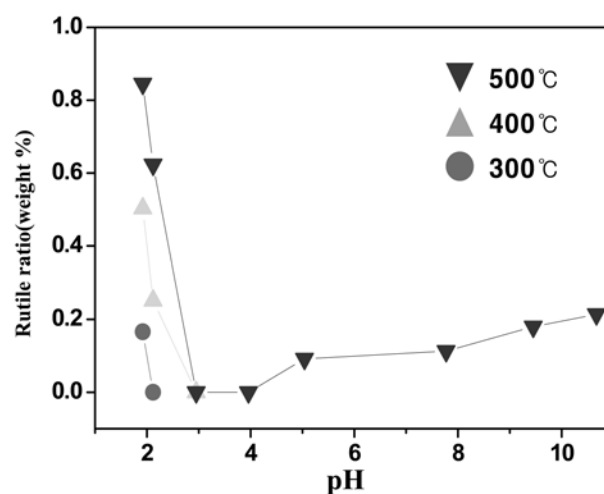


Fig. 5. Calculated rutile weight fractions of the TiO₂ powders as a function of pH.

$$X = 1/(1 + 0.8 I_A/I_R) \quad (3)$$

where,

X ; weight fraction of rutile in the powders

I_A ; X-ray integrated intensity of the strongest peaks of anatase (2θ = 25.3°, (101) plane)

I_R ; X-ray integrated intensity of the strongest peaks of rutile (2θ = 27.5°, (110) plane)

The anatase to rutile transformation is shown as a function of the temperature and pH level in Fig. 5. It is noted that the temperature of the rutile ratio is shifted to a low temperature of 300-400 °C in strong acid. This is attributed to the high surface energy of the particles in strong acid. Therefore, the rutile ratio increases rapidly depending on the lower pH level as well as at higher temperatures, while increases slowly at the higher pH level. It is assumed that the anatase phase has been eliminated following large rutile particles with poor agglomeration, and aggregation takes place during the particle growth process at higher temperatures.

The average crystallite size of the heat-treated powders

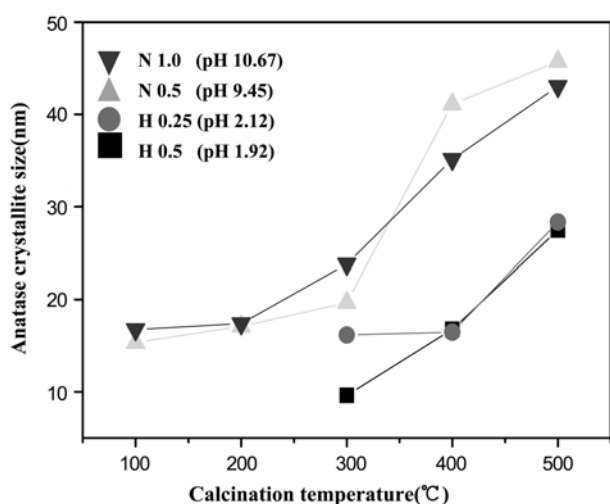


Fig. 6. Average grain size of anatase as a function of calcination temperature.

was calculated using X-ray diffractometry line broadening method through the following Sherrer's equation [47].

$$D = K\lambda/(\beta\cos\theta) \quad (4)$$

where D is the crystallite size, λ is wavelength of the radiation ($\lambda = 1.5418 \text{ \AA}$), θ is Bragg's angle, β is the full width at half maximum (radian) and K is constant (0.9-1.4). Fig. 6 shows the average grain size of anatase as a function of calcination temperature. The average sizes of anatase TiO_2 nanoparticles were in the range of 10-48 nm at calcination temperatures between 100 and 500 °C. Anatase TiO_2 nanoparticles could be obtained above 300 °C in acid (pH 2.12, pH 1.92) with sizes of 10-27 nm, while in the base (pH 10.67, pH 1.92) with sizes 16-47 nm. The anatase nanoparticles could be prepared at a lower temperature in the base solution, and at above 300 °C in the acid solution with a lower particle size compared to the base solution at the same temperature between 300 and 500 °C. It is considered that the remaining amount of anatase became very small in the acid solution, because the phase transformation from anatase to rutile was significantly activated in the acid solution at an increasing temperature. It is noted that nucleation and growth of the rutile phase have been initiated at temperatures from 400-600 °C. Consequently, the phase transformations of amorphous $\text{Ti}(\text{OH})_4$ to anatase TiO_2 and anatase to rutile was significantly activated by the HCl catalyst and temperature. On the other hand, the phase transformation and the crystallization of the powders were not activated by the NH_4OH catalyst.

Conclusions

TiO_2 nanoparticles with a homogeneous particle distribution were successfully prepared using a hydrolysis reaction of titanium tetra-isopropoxide. The morphology and phase transformation of TiO_2 particles prepared by hydrolysis of

titanium tetra-isopropoxide were strongly influenced by the presence of catalysts. In the case of NH_4OH , the morphology of the TiO_2 powder exhibited a powder form. In the case of HCl, it showed a bulk or granular form. The phase transformations of amorphous $\text{Ti}(\text{OH})_4$ to anatase TiO_2 and anatase to rutile were significantly activated by the HCl catalyst. On the other hand, the phase transformation and the crystallization of the particles were not activated by the NH_4OH catalyst.

Acknowledgement

This research was supported by Basic Science Research Program through the National Research Foundation of Korea(NRF) funded by the Ministry of Education, Science and Technology (2010-0023911).

References

1. Y. Zhang, J. Wan and Y. Ke, *J. Hazardous Materials* 177 (2010) 750-754.
2. M.I. Mejia, J.M. Marin, G. Restrepo, L.A. Rios, C. Pulgarin and J. Kiwi, *Applied Catalysis B: Environmental* 94 (2010) 166-172.
3. F. Chen, W. Zou, W. Qu and J. Zhang, *Catalysis Communications* 10 (2009) 1510-1513.
4. J.-H. Li, Y.-Y. Xu, L.-P. Zhu, J.-H. Wang and C.-H. Du, *J. Membrane Science* 326 (2009) 659-666.
5. R. Kaegi, A. Ulrich, B. Sinnet, R. Vonbank, A. Wichser, S. ZSuleeg, H. Simmler, S. Brunner, H. Vonmint, M. Burkhardt and M. Boller, *Environmental Pollution* 156 (2008) 233-239.
6. S. Boujday, F. Wunsch, P. portes, J.-F. Bocquet and C.C. Justin, *Solar Energy Mater. Solar Cells* 83 (2004) 421-433.
7. O. Carp, C.L. Huisman and A. Reller, *Prog. Solid State Chem.* 32 (2004) 133-177.
8. A.M. Ruiz, G. Sakai, A. Cornet, K. Shimanoe, J.R. Morante and N. Yamazoe, *Sens. Actuators B: Chem.* 103 (2004) 312-317.
9. C.J. Barbe, F. Arendse, P. Comte, M. Jirousek and M. Gretzel, *J. Am. Ceram. Soc.* 80 (1997) 3157-3161.
10. R. Monticone, A.V. Tufeu, E. Kanaev and C. Scolan, *Appl. Surf. Sci.* 162-163 (2000) 565-570.
11. Y. Li, X. Sun, H. Li, S. Wang and Y. Wei, *Powder Technology* 194 (2009) 149-152.
12. N. Wetchakun and S. Phanichphant, *Current Applied Physics* 8 (2008) 343-346.
13. B.L. Bischoff and M.A. Anderson, *Chem. Mater.* 7 (1995) 1772-1778.
14. X.-Z. Ding, Z.-Z. Qi and Y.-Z. He, *J. Mater. Sci. Lett.* 14 (1995) 21-22.
15. D. Vorkapic and T. Matsoukas, *J. Am. Ceram. Soc.* 81 (1998) 2815-2820.
16. S. Mahshid, M. Askari and M.S. Ghamsari, *J. Mater. Proc. Tech.* 189 (2007) 296-300.
17. Z. Liu, L. Hong and B. Guo, *J. Powder Sources* 143 (2005) 231-235.
18. K.S. Yoo, T.G. Lee and J. Kim, *Micropo. Mesopo. Mater.* 84 (2005) 211-217.
19. A. Amlouk, L.E. Mir, S. Kraiem and S. Alaya, *J. Phys. Chem. Solids* 67 (2006) 1464-1468.
20. S. Mahshid, M. Askari, M.S. Ghamsari, N. Afshar and S. Lahuti, *J. Alloys and Compounds* 478 (2009) 586-589.

21. Y.T. Kim, Y.S. Park, H. Myung and H.K. Chae, *Colloids Surf. A: Phys. Eng. Asp.* 313-314 (2008) 260-263.
22. C.S. Kim, B.K. Moon, J.H. Park, S.T. Chung and S.M. Son, *J. Cryst. Growth* 254 (2003) 405-410.
23. C.S. Kim, B.K. Moon, J.H. Park, B.C. Choi and H.J. Seo, *ibid.* 257 (2003) 309-315.
24. D. Wang, F. Zhou, C. Wang and W. Liu, *Micropor. Mesopor. Mater.* 116 (2008) 658-664.
25. J. Beusen, M.K. Van Bael, H.V. Rul, J. D'Haen and J. Mullens, *J. Euro. Ceram. Soc.* 27 (2007) 4529-4535.
26. J.K. Oh, J.K. Lee, S.J. Kim and K.W. Park, *J. Ind. Eng. Chem.* 15 (2009) 270-274.
27. D.H. Kim, H.S. Hong, S.J. Kim, J.S. Song and K.S. Lee, *J. Alloys Compd.* 375 (2004) 259-264.
28. P. Xiaoyan and M. Xueming, *Mater. Lett.* 58 (2004) 513-515.
29. J.L. Guimaraes, M. Abbate, S.B. Betim and M.C.M. Alves, *J. Alloys Compd.* 352 (2003) 16-30.
30. M. Kamei and T. Mitsuhashi, *Surf. Sci.* 463 (2000) L609-L612.
31. S. Cassaignon, M. Koelsch and J.-P. Jolivet, *J. Phys. Chem.* 68 (2007) 695-700.
32. A.D. Paola, G. Cufalo, M. Addamo, M. Bellardita, R. Camprostrini, M. Ischia and R. Ceccato, *33. L. Palmisano, Colloids Surf. A: Phys. Eng. Asp.* 317 (2008) 366-376.
33. A.P. Caricato, S. Capone, G. Ciccarella, M. Martino, R. Rella and F. Romano, *J. Spadavecchia*, 35. A. Taurino, T. Tunno, D. Valerini, *Applied Surf. Sci.* 253 (2007) 7937-7941.
34. H. Chang, C.S. Jwo, C.H. Lo, M.J. Kao and S.H. Pai, *J. Alloys Compd.* 434-435 (2007) 668-671.
35. B.L. Bischoff and M.A. Anderson, *Chem. Mater.* 7 (1995) 1772-1778.
36. X.Z. Ding, Z.Z. Qi and Y.Z. He, *J. Mater. Sci. Lett.* 14 (1995) 21-22.
37. D. Vorkapic and T. Matsoukas, *J. Am. Ceram. Soc.* 81 (1998) 2815-2820.
38. J.L. Look and C.F. Zukoski, *ibid.* 75 (1992) 1587-1595.
39. J.L. Look, C.F. Zukoski and C.F. Zukoski, *J. Am. Ceram. Soc.* 78 (1995) 21-32.
40. T. Zeng, Y. Qiu, L. Chen and X. Song, *Mater. Chem. Phys.* 56 (1998) 163-170.
41. T. Sugimoto, X. Zhou and A. Muramatsu, *J. Colloid Interf. Sci.* 259 (2003) 43-52.
42. T. Sugimoto, X. Zhou and A. Muramatsu, *ibid.* 259 (2003) 53-61.
43. J. Livage, M. Henry and C. Sanchez, *Solid State Chem.* 18 (1998) 259-341.
44. H.S. Jung, K.S. Hong and J.K. Lee, *Chem. Lett.* 33 (2004) 1382-1383.
45. N. Phonthammachai, T. Chairassameewong, E. Gulari, A.M. Jamieson and S. Wongkasemjit, *Microporous Mesoporous Mater.* 166 (2003) 261-271.
46. R.A. Spurr and H. Myers, *Anal. Chem.* 29 (1957) 760-762.
47. K.N.P. Kumar, K. Keizer and A.J. Buregraaf, *J. Mat. Chem.* 3 (1993) 1141-1149.